Science of the Total Environment 830 (2022) 154733

Contents lists available at ScienceDirect

Science of the Total Environment

journal homepage: www.elsevier.com/locate/scitotenv

Molecular spectroscopy and docking simulation revealed the binding mechanism of phenol onto anammox sludge extracellular polymeric substances

Gui-Feng Li [a], Zhi-Qi Ren [a], Ye Wang [a], Jing-Peng Li [a], Wen-Jie Ma [a], Ya-Fei Cheng [b], Bao-Cheng Huang [a,*], Ren-Cun Jin [a]

[a] Laboratory of Water Pollution Remediation, School of Life and Environmental Sciences, Hangzhou Normal University, Hangzhou 311121, China
[b] Department of Environmental Science and Engineering, Fudan University, Shanghai 200438, China

HIGHLIGHTS

- Phenol causes the configuration change of anammox sludge EPS.
- Tryptophan proteins dominated the combination with EPS.
- CO functional group of EPS was preferentially responded to phenol.
- The combing process of EPS and phenol was visualized by 3-D molecular simulation.

GRAPHICAL ABSTRACT

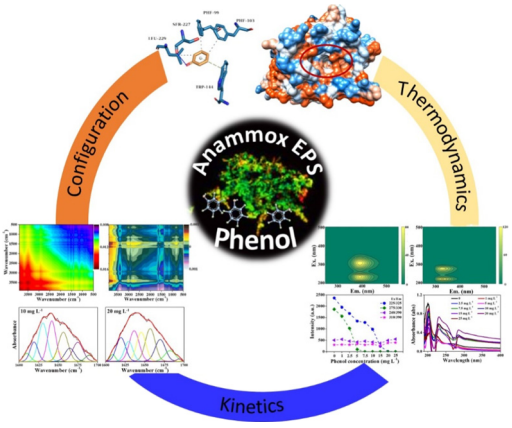

ARTICLE INFO

Article history:
Received 8 January 2022
Received in revised form 27 February 2022
Accepted 17 March 2022
Available online 23 March 2022

Editor: Yifeng Zhang

Keywords:
Anammox
Extracellular polymeric substance
Molecular docking
Phenol

ABSTRACT

The rapid development of chemical industry has induced to the large amount of phenolic wastewater production. When the promising anaerobic ammonium oxidation (anammox) was employed to treat the industrial wastewater, phenolic compounds would possibly inhibit the microbial performance. Extracellular polymeric substances (EPSs) play an essential role in protecting cells from being intoxicated by phenolic compound while the distinct mechanism remains elusive. In this work, the interaction of phenol with anammox sludge EPSs and transmembrane ammonium transport (Amt) domain was explored at molecular level by using spectral method and molecular docking simulation. It was found that phenol statically quenched the fluorescent components of EPSs and the protein component dominated the interaction between EPSs and phenol. The overall interaction was an entropy-driven process with hydrophobic interaction as the main driving force, and the CO vibration responded preferentially. As phenol continued to penetrate into the cell surface, there were hydrogen bond, hydrophobic interaction force and π-π base-stacking forces between the Amt domain and phenol. The interaction between phenol and amino acid residues of the Amt domain would interfere the NH_4^+ transport and further affect the activity of anammox sludge. This work is beneficial for in-depth understanding the role of EPSs in protecting anammox sludge from inhibiting by phenolic pollutants.

* Corresponding author.
E-mail address: huangbc@hznu.edu.cn (B.-C. Huang).

http://dx.doi.org/10.1016/j.scitotenv.2022.154733

1. Introduction

Phenol is an important organic raw material, which has been widely used in the production of many commodities including resins, nylons, plasticizers, additives, medicines, pesticides, dyes and gasoline additives, etc. (Hassan et al., 2018). The growing demand on phenol greatly boosts the relevant industrial development but it also leads to a large amount of phenol-containing wastewater production (Li et al., 2021b). Phenol is a typical toxic phenolic compound, which has been widely found in coking wastewater, pharmaceutical wastewater, sludge digestion liquid and landfill leachate. It has been listed as a priority control pollutant in the United States of America, China, and many other countries (He et al., 2020b). Most of the previous works selected phenol as the model pollutant of industrial wastewater to study its potential ecotoxicity and develop the corresponding removal technology.

To address the deteriorating water environment, the nitrogen content discharged from the industrial wastewater is strictly controlled. As a result, exploring the cost-effective nitrogen removal technology for the above phenol-containing industrial wastewater treatment is meaningful. In the field of biological nitrogen removal, anaerobic ammonium oxidation (anammox) is a promising technology, with few energy requirement and chemical consumption (Li et al., 2019). The application of anammox technology for treatment of industrial wastewater with high ammonia nitrogen, such as coking and petrochemical, has been gradually expanded (Wu et al., 2019; Zhang et al., 2019a). Previous studies have shown that high concentrations of phenol induced a significant toxic effect on anammox sludge. For instance, it was reported that 300 mg L^{-1} phenol deteriorated the anammox bioreactor operation, and the abundance of Ca. Brocadia decreased by 31% (Pereira et al., 2014). Whereas, anammox bioreactor performance was not affected by exposing at 200 mg L^{-1} phenol (Pereira et al., 2014; Zhou et al., 2020). Different sludge morphologies, i.e., suspended or granular, would result in a different half inhibitory concentration of phenol (Peng et al., 2018; Yang et al., 2013). Under the phenol stress, anammox sludge would largely excrete extracellular polymeric substances (EPSs) to sustain cell activity (Wang et al., 2019). Nevertheless, the exact role and response mechanism of anammox EPSs to phenol still remains elucidated.

Previous studies have shown that the amount of EPSs excreted by anammox sludge was higher than that of activated sludge (Hou et al., 2015) and protein was a predominant component of anammox sludge EPSs (Boleij et al., 2018; Jia et al., 2017). Among the extracellular proteins, researchers have found that hydrophobic amino acids are the main components (Jia et al., 2017; Sun et al., 2018). The above hydrophobic groups in EPSs are possible to interact with lipophilic aromatic compound, thereby reducing the potential toxicity of phenol to anammox sludge. However, the details on the role of anammox sludge EPSs and its structural change under phenol stress are not yet known, and it is also not clear on what happens when phenol contacts with membrane proteins.

Here, this work aims to unveil the binding mechanism between anammox sludge EPSs and phenol based on the spectral analysis method from the perspectives of kinetics, thermodynamics and configuration change. What's more, a three-dimensional molecular structure diagram of the interaction between the transmembrane ammonium transport (Amt) domain and phenol was obtained through molecular simulation technology. This work is beneficial to better understanding the role of EPSs in protecting microorganisms from toxic pollutants in the anammox system. It also provides theoretical support for in-depth understanding the stability of anammox sludge under the stress of phenolic compounds.

2. Materials and methods

2.1. Anammox sludge EPSs sources and its binding with phenol

Anammox granular sludge has been successfully enriched in a lab-scale upflow anaerobic sludge blanket reactor. The dominant bacterium in the enriched anammox sludge is Ca. Kuenenia (49.09%). The detailed information was shown in our previous work (Li et al., 2020b). The heating method was used to extract EPSs from anammox sludge, as reported by He et al. (2020a). Briefly, the anammox sludge washed three times with 0.9% NaCl was heat-treated at 80 °C for 1 h, and then centrifuged at 8000 rpm for 15 min, and the supernatant was the total EPSs. The extracted total EPSs was filtered through the 0.45 μm membrane and quantified through a total organic carbon (TOC) analyzer (Multi N/C 2100, Analytik Jena, Germany).

To probe the potential influence of phenol on EPSs structural change, a batch shaking flask experiment was conducted. In brief, EPSs (100 mg TOC L^{-1}) was mixed with phenol in a series of concentrations (0–25 mg L^{-1}) to a final volume of 25 mL. Each group of EPSs-phenol mixture was placed in a shaker at 35 °C, and oscillated at 150 rpm for 24 h to reach equilibrium. The obtained EPSs-phenol sample was subjected to subsequent determination and analysis.

2.2. Sample spectra collection and chemical analysis

Ultraviolet (UV) absorption spectra were obtained using a dual beam spectrophotometer (UV-4500, Shimadzu Co., Japan). The UV differential spectrum (190–400 nm) of the EPSs-phenol mixture was obtained by using phenol solution as a reference. The linear regression based on $1/(A\text{-}A_0)$ and $1/C$ was then carried out to obtain the binding constant, according to the double reciprocal formula (Text S1). The synchronous fluorescence spectra were collected by a fluorescence spectrophotometer (F-4600, Hitachi Co., Japan), with scanning wavelength from 200 to 500 nm. The interval of excitation and emission were 60 and 100 nm, respectively. Additionally, three-dimensional fluorescence excitation emission matrix (EEM) spectra were collected. Due to the severe overlap of fluorescence spectrum, parallel factor (PARAFAC) analysis was performed to decompose EEM spectrum to obtain effective spectral information (Zhang et al., 2019b). Furthermore, the freeze-dried EPSs or EPSs-phenol samples were mixed with KBr for Fourier transform infrared (FTIR) spectroscopy scanning after grinding. Two-dimensional correlation spectroscopy (2DCOS) analysis was performed by using FTIR data, according to our previous work (Li et al., 2020b).

The method for determination of polysaccharide, protein, and humic acid in EPSs was same as in our previous report (Li et al., 2020a). The zeta potential of EPSs-phenol mixture was measured using Nanosize ZS potentiometer (Malvern Instrumens Co., UK). Three parallel measurements were performed for each test. One-way ANOVA was used to analyze the difference between the two groups. The significant difference was defined as $p < 0.05$ and the extremely significant difference was defined as $p < 0.01$.

2.3. Molecular docking simulation

Considering that phenol continuously penetrates inward, it is inevitable to contact with anammox cell membrane proteins. The Amt domain of anammox bacterium was selected for molecular docking with phenol, and the crystal structure has been deconstructed by Pflüger et al. (2018), which could be acquired from the Protein Data Bank (PDB ID: 6EU6). The steepest descent method was applied to minimize the energy of the Amt domain to eliminate the close contact between atoms. The 3D structure of phenol was acquired from the PubChem database (Compound CID: 108-95-2). Chem3D 14.0 was used to optimize the energy minimization. The molecular docking simulation between Amt domain and phenol was conducted by AutoDock (version 4.2.6) (Morris et al., 2009). 1000 conformations were searched, and the conformation with the lowest energy was selected as the optimal binding conformation. Chimera 1.13.1 and PyMOL 2.1 were used to analyze the hydrophobic properties and electrostatic potential of the protein-ligand, respectively. The interaction between the receptor and the ligand was analyzed via the fully automated protein–ligand interaction profiler, an online server (https://plip-tool.biotec.tu-dresden.de/plip-web/plip) (Salentin et al., 2015).

3. Results and discussion

3.1. The binding property of phenol onto anammox EPSs

The components of anammox EPSs are shown in Table S1. The proteins/polysaccharides ratio was 5.8. Apparently, proteins were the main component of EPSs, which is consistent to other studies (Guo et al., 2017; He et al., 2020a; Sun et al., 2018; Yin et al., 2015). The zeta potential of EPSs-phenol mixture are shown in Table S2. The addition of 1 mg L^{-1} phenol had a significant reduction ($p < 0.01$) in the absolute value of negative zeta potential (from −14.2 mV to −2.43 mV). The absolute value of negative zeta potential gradually increased with the phenol concentration increasing to 10 mg L^{-1}, but it was always lower than the initial value. Until the 20 mg L^{-1} phenol was added, the absolute value of negative zeta potential exceeded the pristine EPSs (−15.9 mV). Phenol mainly existed in the form of molecules under neutral pH conditions (Dąbrowski et al., 2005). As a consequence, the reduction in the absolute value of negative zeta potential was mainly due to configuration change rather than charge neutralization.

The binding constant between phenol and EPSs was probed by UV differential absorption spectroscopy. The spectral segments at 190–400 nm could well represent the information of EPSs. Fig. 1a showed that the absorbance of EPSs near 200 nm decreased with the addition of phenol, and the absorption wavelength was redshifted. As previously reported, this was mainly caused by the π-π* transition of CO in the peptide bond (Oladepo et al., 2011). The binding constant of phenol and EPSs (K, M^{-1}) was calculated according to the double reciprocal formula (Purcell et al., 2000) (Text S1). Based on the linear regression result, the binding constant between phenol and anammox sludge EPSs was estimated as 17,348.25 M^{-1} (35 °C).

The interaction forces between phenol and EPSs may include hydrophobic interactions, hydrogen bonds, van der Waals force and/or electrostatic force. It can be determined according to the thermodynamic parameters of the reaction. Enthalpy change (ΔH) can approximate to be constant within a small temperature range (Yang et al., n.d.). The entropy-changing (ΔS, kJ mol^{-1} K^{-1}) and free energy (ΔG, kJ mol^{-1}) can then be estimated according to the thermodynamic parameter relations (Text S2). The thermodynamic function value of the combination of phenol and EPSs was calculated as ΔH = 147.39 KJ mol^{-1}; ΔS = 0.559 KJ mol^{-1} K^{-1} (35 °C), 0.559 KJ mol^{-1} K^{-1} (25 °C); and ΔG = −25.01 KJ mol^{-1} (35 °C), −19.41 KJ mol^{-1} (25 °C). $\Delta H > 0$, $\Delta G < 0$, showed that the combination of phenol with EPSs was a spontaneous endothermic reaction. $\Delta S > 0$, $|\Delta H| < |T\Delta S|$, illustrated that the disorder degree of the system increased (Hu et al., 2009). The above results imply that the combination of EPSs and phenol was an entropy driven process, with hydrophobic interaction as the main driving force.

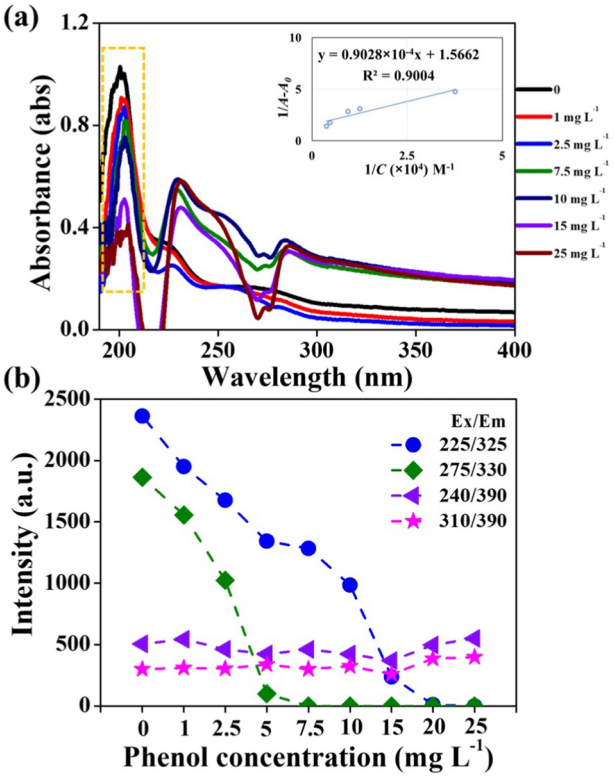

Fig. 1. The UV differential absorption spectrum of EPSs with the linear regression of the binding constant according to the double reciprocal formula at different concentrations of phenol (a), and the change of fluorescence intensity decomposed by PARAFAC (b).

3.2. Fluorescence quenching mechanism

Through analyzing with PARAFAC, the EEM spectrum of EPSs can be decomposed into two major fluorescent components, i.e., protein-like (Component 1) and humic acid-like (Component 2) substances (Xiao et al., 2007). The excitation/emission of the two fluorescent components was 225/275, 325 nm (Component 1) and 240, 310/390 nm (Component 2) (Fig. S1). The aromatic proteins at 225/325 nm showed the highest fluorescence intensity, followed by tryptophan proteins at 275/325 nm and humic acids at 240/390 nm. The differential spectra of EEM showed that the main fluorescence components of EPSs obviously changed after the addition of phenol. Phenol could result in a typical fluorescence quenching phenomenon (Fig. 1b), suggesting its strong interaction with EPSs.

To further explore the fluorescence quenching type of EPSs by phenol, both the fluorescence quenching constant (K_{sv}, M^{-1}) and quenching rate constant (k_q, M^{-1} s^{-1}) were calculated by Stern-Volmer formula (Text S3). Table 1 showed that the kq of three main fluorescence substances all higher than 2×10^{10} M^{-1} s^{-1}, indicating a possible static quenching process (Bi et al., 2005). In other words, phenol combined with EPSs to form a non-fluorescent complex, which leads to fluorescence quenching. Also, the quenching constant of proteins was found to be the largest, which signified that proteins might dominate the interaction between EPSs and phenol. Indeed, our previous proteomic analysis of anammox EPSs revealed that there are a large number of proteins related to binding, transport, and outer-membrane cell components, etc. (Li et al., 2021a).

3.3. Phenol affects the conformation of EPSs

The synchronous fluorescence spectra of tryptophan and aromatic protein can be obtained via setting the excitation-emission interval ($\Delta\lambda$) of 60 nm and 100 nm, respectively (Fig. 2). It was found that the synchronous fluorescence quenching of EPSs was obvious with the addition of phenol. Besides, the maximum emission wavelength was redshifted, indicating that phenol clearly affected the conformation of EPSs. The polarity near the fluorophore was enhanced and the hydrophobicity decreased (Deng et al., 2017). To further characterize the priority response order of functional groups and the secondary structure change of proteins under phenol stress, FTIR spectroscopy was further analyzed (Fig. 2c).

The FTIR spectra showed that it mainly involved the OH stretching with hydrocarbons (3410 cm^{-1}), the CO vibration associated with protein amide I (1639 cm^{-1}), the CO symmetric stretching of COO in amide II (1402 cm^{-1}), COH and CO with polysaccharide (1145 cm^{-1}), and OPO

Table 1
The Stern-Volmer quenching constant and quenching rate constant of the main fluorescent substance in EPSs after interacting with phenol.

Fluorescence component	K_{sv} (M^{-1})	k_q (M^{-1} s^{-1})	R^2
Aromatic protein	1.24×10^4	1.24×10^{12}	0.9508
Tryptophan protein	2.92×10^4	2.92×10^{12}	0.9246
Humic acid	0.20×10^3	0.20×10^{11}	0.8408

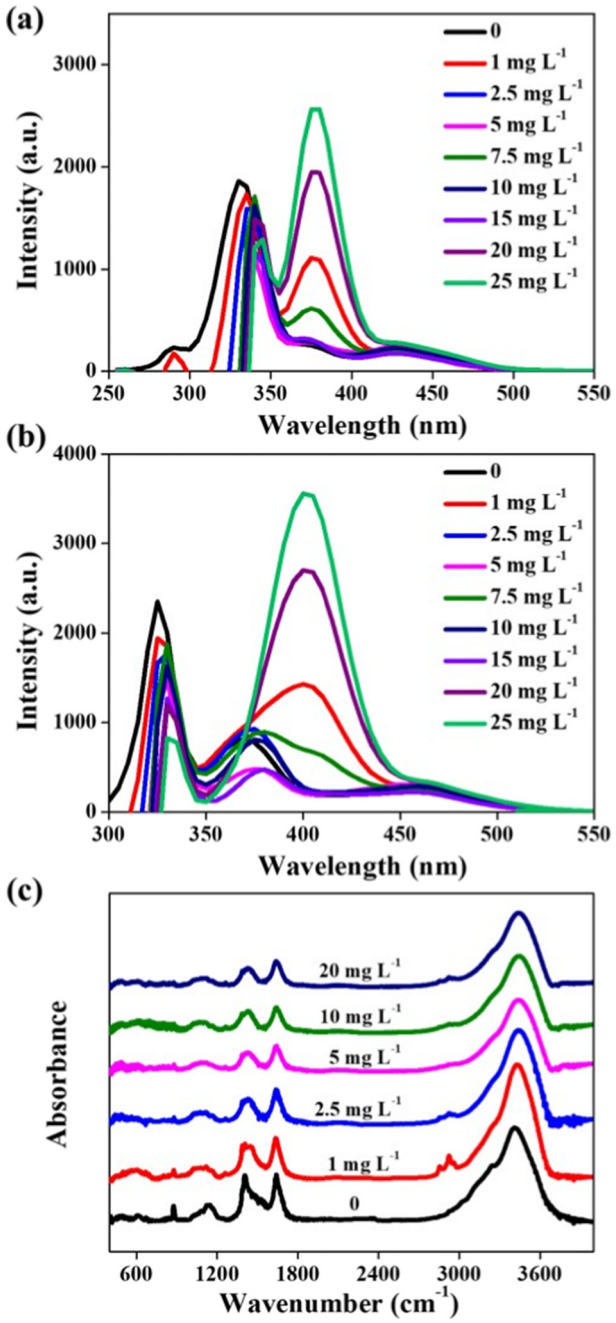

Fig. 2. Synchronous fluorescence spectra of the EPSs under phenol disturbance (a: $\Delta\lambda$ = 60 nm, b: $\Delta\lambda$ = 100 nm), and the FTIR absorbance spectra of the freeze-dried EPSs samples (c).

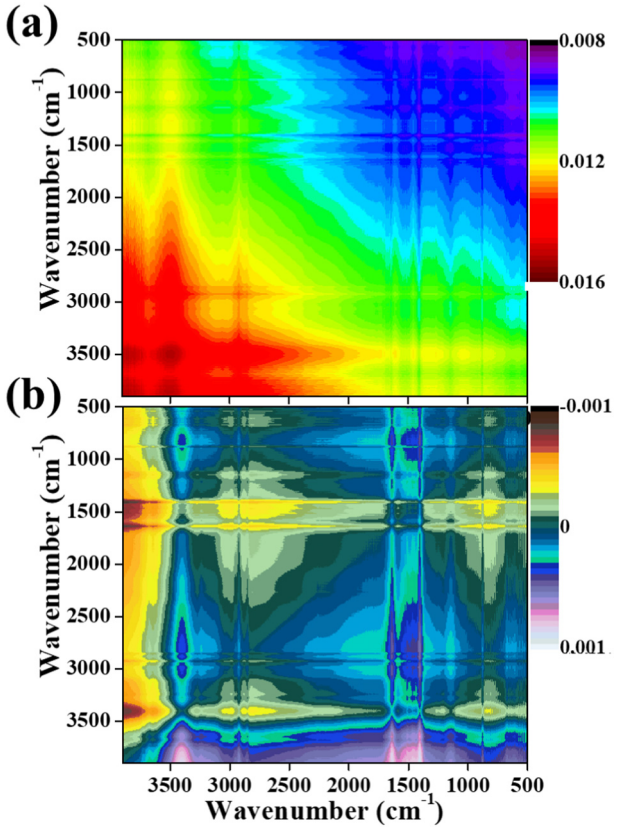

Fig. 3. The obtained FTIR synchronous (a) and asynchronous (b) spectra of EPSs under phenol disturbance from 2DCOS analysis.

stretch associated with nucleic acid (875 cm^{-1}) (Wang et al., 2020). The precedence response order of the different groups under phenol disturbance was studied by 2DCOS analysis (Fig. 3). In the synchronous spectrum of 2DCOS, there were 5 autocorrelation peaks located near 3410, 1640, 1400, 1145 and 875 cm^{-1} (Fig. 3). Their cross correlation peaks were all positive, indicating that their changes were consistent. The signs of the cross-correlation peaks in the asynchronous spectrum are shown in Table 3. The sequence of group changes in EPSs under phenol disturbance was 1640 > 3410 > 1400 > 1145 > 875 cm^{-1} according to the order rule (Chen et al., 2015; Chen et al., 2019a). Protein-related groups was found to preferentially interact with phenol.

The amide I band ranged at1600–1700 cm^{-1} was then analyzed (Fig. S2) (Yin et al., 2015) and the relative content of the different protein structures was shown in Table 2. The addition of phenol changed the secondary structure of proteins in the EPSs, and the most obvious was that the content of β-sheets decreased, while the content of random coils increased. The ratio of α-helix/(β-sheet + random coil) was commonly adopted to reflect the tightness of protein structure. An increased ratio was observed with the addition of phenol, implying that the overall structure of EPSs protein became compact. Proteins with denser structures may expose fewer internal hydrophobic groups (Wang et al., 2012). The reduction of the internal hydrophobic point may not be conducive to the subsequent binding of phenol.

3.4. Molecular docking simulation analysis

As phenol continuously migrates into the EPSs and penetrates to the cell surface, it is inevitable to contact with membrane proteins. The molecular docking structure diagram was obtained by using molecular simulation technology to intuitively understand the interaction between phenol and

Table 2
Band assignments for the protein secondary structures of EPSs after exposing to different concentrations of phenol.

Secondary structures	At. %			
	Phenol concentration (mg L^{-1})			
	0	2.5	10	20
β-Sheet	60.39 ± 1.03	47.17 ± 2.65	48.19 ± 1.54	51.13 ± 2.68
Random coil	6.52 ± 2.11	22.20 ± 1.32	13.86 ± 2.36	16.12 ± 1.86
α-Helix	15.67 ± 1.36	19.47 ± 1.89	17.69 ± 2.09	19.35 ± 2.31
β-Turn	17.42 ± 1.25	11.15 ± 2.14	20.26 ± 3.01	13.40 ± 1.99
α-Helix/(β-sheet + random coil)	0.23 ± 0.55	0.28 ± 0.04	0.29 ± 0.07	0.29 ± 0.05

Table 3
2DCOS results on the sign of each cross-peak in synchronous and asynchronous maps of EPS-phenol mixture.

Position	Sign				
nm	3409	1639	1402	1145	875
3409	+	+(−)	+(+)	+(+)	+(+)
1639		+	+(+)	+(+)	+(+)
1402			+	+(−)	+(+)
1145				+	+(+)
875					+

protein. Ammonium transporter is an important transmembrane protein of anammox, involving in the transportation of NH_4^+ from outside to inside the cell (Chen et al., 2019b; Pflüger et al., 2018). Fig. 4 showed the molecular docking simulation of Amt domain and phenol. The minimum binding free energy of the two was -4.66 kcal mol^{-1} and the interaction forces between phenol and Amt domain include hydrogen bonds, hydrophobic forces and π-π base-stacking forces. The amino acid residue involved in the formation of hydrogen bonds was Ser-227. At the same time, there were hydrophobic interactions between aromatic amino acid residues Phe-99, Phe-103, Leu-229 and the phenol. The π-π base-stacking forces mainly existed between the aromatic amino acid Trp-144 and phenol. Among them, Ser-227, Phe-103 and Trp-144 were located on the NH_4^+ channel (Pflüger et al., 2018), and the changes in these amino acid residues may affect the NH_4^+ transport.

3.5. Effects of external disturbances on the interaction between EPSs and phenol

EPSs play an indispensable role during resistance of anammox sludge to phenol poisoning. Unpredictable factors inevitably lead to the living environment fluctuations of anammox sludge during the bioreactor operation. Herein, the effects of external disturbances, such as temperature and pH changes, on the interaction between EPSs and phenol were further investigated. Phenol showed the strongest interaction with anammox sludge EPSs at 35 °C, as evidenced by the highest binding constant (17,348.25 M^{-1}, R^2 = 0.9004). The binding strength was weakened as the temperature decreased, and the binding constants were 2516.41 M^{-1} (R^2 = 0.9952), and 2207.02 M^{-1} (R^2 = 0.9989) at 25 °C and 15 °C, respectively. It is worth noting that the binding constant at 35 °C was 6.9 times higher than that of 25 °C, which is more significant than the difference between 25 °C and 15 °C. Wang et al. (2019) investigated the effect of phenol on mainstream anammox sludge and they found that 35 mg L^{-1} phenol severely inhibited anammox activity at low temperature (20 °C). The threshold concentration of phenol on anammox sludge is reduced at low temperature compared to 35 °C. According to our result, this may be due to the weakened binding ability of EPSs to phenol at low temperature.

The influence of different pH conditions on binding phenol was investigated (Table S3). The binding constant was the largest in neutral and weakly alkaline environment. An acidic or alkaline environment at pH > 8 can adversely affect the combination. This may be due to the stronger compression and compact structure of EPSs in acidic environments, and simultaneously the electrostatic repulsion increased in the alkaline environment. Nevertheless, EPSs had more extended chain structure in neutral and weakly alkaline environment, which was conducive to take function with phenol (Wang et al., 2012).

4. Conclusions

In this study, the interaction of phenol with anammox sludge EPSs and transmembrane Amt domain were revealed through spectroscopic analysis and molecular simulation technique. The combining of anammox sludge EPSs and phenol was an entropy driven process with hydrophobic interaction as the main driving force, and the protein component played a leading role in the binding process. Under the phenol stress, the CO vibration responded preferentially over other functional groups within the EPSs. The secondary structure of the protein in EPSs changed and became more compact due to the entry of phenol, which resulted in fewer exposed internal hydrophobic points and was not conducive to subsequent phenol binding. As phenol continuously migrates into the EPSs and penetrates to the cell surface, it interacted with amino acid residues of Amt domain such as Ser-227, Phe-103 and Trp-144, located on the NH_4^+ channel, through hydrogen bond, hydrophobic interaction force and π-π base-stacking forces. The above combination might adversely affect the transport of NH_4^+ by anammox sludge. The results of this work will help to better understand the behavior of phenol in anammox sludge when treating phenol-containing industrial wastewater.

CRediT authorship contribution statement

Gui-Feng Li: Investigation, Methodology, Data Curation, Software, Writing - Original Draft.
Zhi-Qi Ren: Methodology, Investigation.
Ye Wang: Investigation, Data Curation.
Jing-Peng Li: Data Curation, Validation.
Wen-Jie Ma: Methodology, Visualization.
Ya-Fei Cheng: Investigation, Software.
Bao-Cheng Huang: Conceptualization, Formal analysis, Review & Editing, Supervision.
Ren-Cun Jin: Review & Editing, Project administration, Funding acquisition.

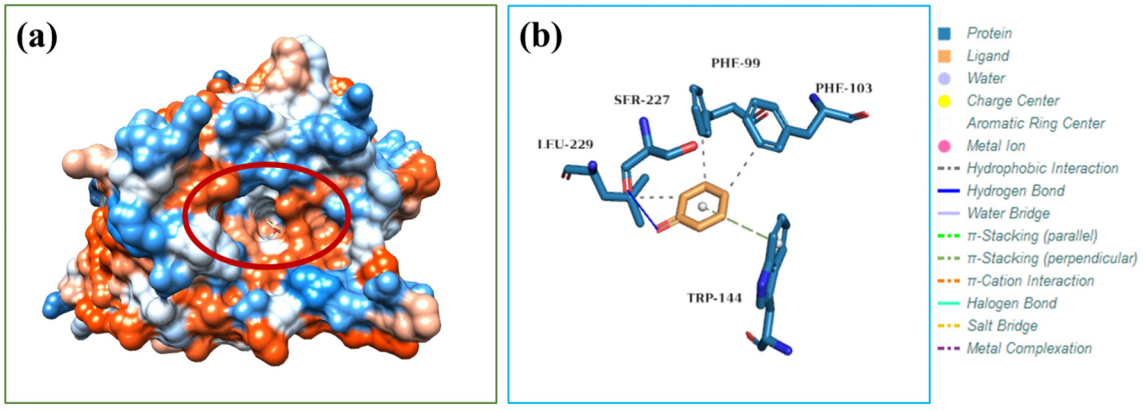

Fig. 4. Molecular docking simulation of the interaction between Amt domain and phenol. (a) The polarity analysis of the binding area. The orange area represented the strong hydrophobicity of the protein, and the blue area represented the strong hydrophilicity. (b) The interaction force between them, including hydrogen bond, hydrophobic forces and π-π base-stacking forces. PHE: phenylalanine; TRP: tryptophan; SER: serine; LEU: leucine.

Declaration of competing interest

The authors declare that they have no known competing financial interests or personal relationships that could have appeared to influence the work reported in this paper.

Acknowledgments

The authors wish to thank the National Natural Science Foundation of China (51878231) for the partial support of this study.

Appendix A. Supplementary data

Supplementary data to this article can be found online at https://doi.org/10.1016/j.scitotenv.2022.154733.

References

Bi, S., Song, D., Tian, Y., Zhou, X., Liu, Z., Zhang, H., 2005. Molecular spectroscopic study on the interaction of tetracyclines with serum albumins. Spectrochim. Acta A Mol. Biomol. Spectrosc. 61 (4), 629–636.

Boleij, M., Pabst, M., Neu, T.R., van Loosdrecht, M.C., Lin, Y., 2018. Identification of glycoproteins isolated from extracellular polymeric substances of full-scale anammox granular sludge. Environ. Sci. Technol. 52 (22), 13127–13135.

Chen, W., Habibul, N., Liu, X.-Y., Sheng, G.-P., Yu, H.-Q., 2015. FTIR and synchronous fluorescence heterospectral two-dimensional correlation analyses on the binding characteristics of copper onto dissolved organic matter. Environ. Sci. Technol. 49 (4), 2052–2058.

Chen, W., Teng, C.-Y., Qian, C., Yu, H.-Q., 2019a. Characterizing properties and environmental behaviors of dissolved organic matter using two-dimensional correlation spectroscopic analysis. Environ. Sci. Technol. 53 (9), 4683–4694.

Chen, Z., Meng, Y., Sheng, B., Zhou, Z., Jin, C., Meng, F., 2019b. Linking exoproteome function and structure to anammox biofilm development. Environ. Sci. Technol. 53 (3), 1490–1500.

Dąbrowski, A., Podkościelny, P., Hubicki, Z., Barczak, M., 2005. Adsorption of phenolic compounds by activated carbon—a critical review. Chemosphere 58 (8), 1049–1070.

Deng, S., Zeng, D., Luo, Y., Zhao, J., Li, X., Zhao, Z., Chen, T., 2017. Enhancement of cell uptake and antitumor activity of selenadiazole derivatives through interaction and delivery by serum albumin. RSC Adv. 7 (27), 16721–16729.

Guo, Y., Liu, S., Tang, X., Yang, F., 2017. Role of c-di-GMP in anammox aggregation and systematic analysis of its turnover protein in Candidatus Jettenia caeni. Water Res. 113, 181–190.

Hassan, H., Jin, B., Donner, E., Vasileiadis, S., Saint, C., Dai, S., 2018. Microbial community and bioelectrochemical activities in MFC for degrading phenol and producing electricity: microbial consortia could make differences. Chem. Eng. J. 332, 647–657.

He, C.-S., Ding, R.-R., Chen, J.-Q., Li, W.-Q., Li, Q., Mu, Y., 2020a. Interactions between nanoscale zero valent iron and extracellular polymeric substances of anaerobic sludge. Water Res. 115817.

He, Q., Xie, Z., Fu, Z., Wang, H., Chen, L., Gao, S., Zhang, W., Song, J., Xu, P., Yu, J., 2020b. Effects of phenol on extracellular polymeric substances and microbial communities from aerobic granular sludge treating low strength and salinity wastewater. Sci. Total Environ. 752, 141785.

Hou, X., Liu, S., Zhang, Z., 2015. Role of extracellular polymeric substance in determining the high aggregation ability of anammox sludge. Water Res. 75, 51–62.

Hu, Y.-J., Liu, Y., Xiao, X.-H., 2009. Investigation of the interaction between berberine and human serum albumin. Biomacromolecules 10 (3), 517–521.

Jia, F., Yang, Q., Liu, X., Li, X., Li, B., Zhang, L., Peng, Y., 2017. Stratification of extracellular polymeric substances (EPS) for aggregated anammox microorganisms. Environ. Sci. Technol. 51 (6), 3260–3268.

Li, G.-F., Huang, B.-C., Zhang, Z.-Z., Cheng, Y.-F., Fan, N.-S., Jin, R.-C., 2019. Recent advances regarding the impacts of engineered nanomaterials on the anaerobic ammonium oxidation process: performances and mechanisms. Environ. Sci. Nano 6 (12), 3501–3512.

Li, G.-F., Huang, B.-C., Cheng, Y.-F., Ma, W.-J., Li, S.-T., Gong, B., Guan, Y.-F., Fan, N.-S., Jin, R.-C., 2020a. Determination of the response characteristics of anaerobic ammonium oxidation bioreactor disturbed by temperature change with the spectral fingerprint. Sci. Total Environ. 719, 137513.

Li, G.-F., Ma, W.-J., Cheng, Y.-F., Li, S.-T., Zhao, J.-W., Li, J.-P., Liu, Q., Fan, N.-S., Huang, B.-C., Jin, R.-C., 2020b. A spectra metrology insight into the binding characteristics of Cu2+ onto anammox extracellular polymeric substances. Chem. Eng. J. 393, 124800.

Li, G.-F., Ma, W.-J., Ren, Z.-Q., Wang, Y., Li, J.-P., Zhao, J.-W., Li, S.-T., Liu, Q., Gu, Y.-N., Cheng, Y.-F., 2021a. Molecular insight into the binding property and mechanism of sulfamethoxazole to extracellular proteins of anammox sludge. Environ. Sci. Technol. 55 (24), 16627–16635.

Li, Z., Wei, C., Chen, Y., Chen, B., Qiu, G., Wan, J., Wu, H., Zhu, S., Zhao, H., 2021b. Achieving nitritation in an aerobic fluidized reactor for coking wastewater treatment: operation stability, mechanisms and model analysis. Chem. Eng. J. 406, 126816.

Morris, G.M., Huey, R., Lindstrom, W., Sanner, M.F., Belew, R.K., Goodsell, D.S., Olson, A.J., 2009. AutoDock4 and AutoDockTools4: automated docking with selective receptor flexibility. J. Comput. Chem. 30 (16), 2785–2791.

Oladepo, S.A., Xiong, K., Hong, Z., Asher, S.A., 2011. Elucidating peptide and protein structure and dynamics: UV resonance Raman spectroscopy. J. Phys. Chem. Lett. 2 (4), 334–344.

Peng, S., Han, X., Song, F., Zhang, L., Wei, C., Lu, P., Zhang, D., 2018. Inhibition of benzene, toluene, phenol and benzoate in single and combination on anammox activity: implication to the denitrification–anammox synergy. Biodegradation 29 (6), 567–577.

Pereira, A.D., Leal, C.D., Dias, M.F., Etchebehere, C., Chernicharo, C.A.L., de Araújo, J.C., 2014. Effect of phenol on the nitrogen removal performance and microbial community structure and composition of an anammox reactor. Bioresour. Technol. 166, 103–111.

Pflüger, T., Hernández, C.F., Lewe, P., Frank, F., Mertens, H., Svergun, D., Baumstark, M.W., Lunin, V.Y., Jetten, M.S., Andrade, S.L., 2018. Signaling ammonium across membranes through an ammonium sensor histidine kinase. Nat. Commun. 9 (1), 1–11.

Purcell, M., Neault, J., Tajmir-Riahi, H., 2000. Interaction of taxol with human serum albumin. Biochim. Biophys. Acta Protein Struct. Mol. Enzymol. 1478 (1), 61–68.

Salentin, S., Schreiber, S., Haupt, V.J., Adasme, M.F., Schroeder, M., 2015. PLIP: fully automated protein–ligand interaction profiler. Nucleic Acids Res. 43 (W1), W443–W447.

Sun, Y., Guan, Y., Zeng, D., He, K., Wu, G., 2018. Metagenomics-based interpretation of AHLs-mediated quorum sensing in anammox biofilm reactors for low-strength wastewater treatment. Chem. Eng. J. 344, 42–52.

Wang, L.-L., Wang, L.-F., Ren, X.-M., Ye, X.-D., Li, W.-W., Yuan, S.-J., Sun, M., Sheng, G.-P., Yu, H.-Q., Wang, X.-K., 2012. pH dependence of structure and surface properties of microbial EPS. Environ. Sci. Technol. 46 (2), 737–744.

Wang, G., Dai, X., Zhang, D., 2019. Effects of NaCl and phenol on anammox performance in mainstream reactors with low nitrogen concentration and low temperature. Biochem. Eng. J. 147, 72–80.

Wang, W., Yan, Y., Zhao, Y., Shi, Q., Wang, Y., 2020. Characterization of stratified EPS and their role in the initial adhesion of anammox consortia. Water Res. 169, 115–233.

Wu, L., Shen, M., Li, J., Huang, S., Li, Z., Yan, Z., Peng, Y., 2019. Cooperation between partial-nitrification, complete ammonia oxidation (comammox), and anaerobic ammonia oxidation (anammox) in sludge digestion liquid for nitrogen removal. Environ. Pollut. 254, 112965.

Xiao, J., Shi, J., Cao, H., Wu, S., Ren, F., Xu, M., 2007. Analysis of binding interaction between puerarin and bovine serum albumin by multi-spectroscopic method. J. Pharm. Biomed. Anal. 45 (4), 609–615.

Yang, G.-F., Guo, X.-L., Chen, S.-X., Liu, J.-H., Guo, L.-X., Jin, R.-C., 2013. The evolution of anammox performance and granular sludge characteristics under the stress of phenol. Bioresour. Technol. 137, 332–339.

Yang et al., n.d. J. Yang S.-C. Huang Y. Wang M.-Y. Ji Y.-J. Hu, Multispectroscopic, electrochemical and molecular docking approaches on binding comparison of Camptothecin, 10-Hydroxycamptothecin to bovine serum albumin. J. Mol. Liq., 115296.

Yin, C., Meng, F., Chen, G.-H., 2015. Spectroscopic characterization of extracellular polymeric substances from a mixed culture dominated by ammonia-oxidizing bacteria. Water Res. 68, 740–749.

Zhang, F., Peng, Y., Wang, S., Wang, Z., Jiang, H., 2019a. Efficient step-feed partial nitrification, simultaneous anammox and denitrification (SPNAD) equipped with real-time control parameters treating raw mature landfill leachate. J. Hazard. Mater. 364, 163–172.

Zhang, Z.-Z., Cheng, Y.-F., Liu, Y.-Y., Zhang, Q., Zhu, B.-Q., Jin, R.-C., 2019b. Deciphering the evolution characteristics of extracellular microbial products from autotrophic and mixotrophic anammox consortia in response to nitrogen loading variations. Environ. Int. 124, 501–510.

Zhou, X., Wang, G., Yin, Z., Chen, J., Song, J., Liu, Y., 2020. Performance and microbial community in a single-stage simultaneous carbon oxidation, partial nitritation, denitritation and anammox system treating synthetic coking wastewater under the stress of phenol. Chemosphere 243, 125382.